AIAA Aviation Forum and ASCEND co-located Conference Proceedings
21 - 25 July 2025, Las Vegas, Nevada
AIAA AVIATION FORUM AND ASCEND 2025

10.2514/6.2025-3454

Spectral proper orthogonal decomposition of transitional flow over an open cavity

Felipe O. Aguirre *
University of São Paulo, São Carlos, São Paulo, 13563-120, Brazil

Oliver T. Schmidt†
University of California San Diego, La Jolla, CA 92093, USA

Marcello A. F. Medeiros ‡
University of São Paulo, São Carlos, São Paulo, 13563-120, Brazil

This study investigates boundary layer transition over an open cavity under subsonic flow conditions, motivated by the economic and environmental impact of reducing aerodynamic drag. Using Direct Numerical Simulation (DNS), Linear Stability Theory (LST), and Spectral Proper Orthogonal Decomposition (SPOD), the research examines how cavity-induced instabilities, such as Rossiter (acoustic feedback-driven) and centrifugal modes, interact to drive transition, building on prior work linking surface imperfections to bypass transition mechanisms. Results reveal nonlinear couplings between these modes, with Rossiter modes persisting into turbulent regions and centrifugal instabilities introducing three-dimensional flow distortions, highlighting their combined role in destabilizing the boundary layer.

I. Nomenclature

C_n	=	Centrifugal mode n
D	=	Cavity depth
f	=	Frequency
L	=	Cavity length
M	=	Mach number
N	=	T-S spatial amplification ratio
C_f	=	Friction Coefficient
R_n	=	Rossiter mode n
Re_D	=	Reynolds number based on cavity depth
Re_L	=	Reynolds number based on cavity length
Re_{δ^*}	=	Reynolds number based on displacement thickness
T-S	=	Tollmien-Schlichting wave
U_∞	=	Free-stream velocity
X	=	Stream-wise distance normalized by displacement thickness
Y	=	Wall-normal distance normalized by displacement thickness
β	=	Span-wise wave number
δ^*	=	Displacement thickness
λ	=	Span-wise wavelength
σ	=	Amplification rate
ω	=	Frequency

*PhD student, São Carlos School of Engineering, University of São Paulo, Av. João Dagnone, 1100, São Carlos/SP - Brazil,
†Associate Professor, Department of Mechanical and Aerospace Engineering, Senior Member AIAA.
‡Professor, São Carlos School of Engineering, University of São Paulo, Av. João Dagnone, 1100, São Carlos/SP - Brazil

II. Introduction

The shear forces in the boundary layer are characteristic of dissipative behavior. Specifically, in an aircraft, these forces contribute to drag in the form of viscous skin friction. Moreover, a turbulent boundary layer significantly increases drag. Consequently, engineering has an economic interest in studying transition. To illustrate the economic and environmental impact, Schneider [1] quantified that a hypothetical 1% reduction in total aerodynamic drag of a large commercial aircraft operating over long distances would result in fuel savings of 400, 000 liters and a reduction of 5, 000 kg in harmful gas emissions per year. Additionally, Marec [2] stated that approximately 50% of the total drag of a typical civil transport aircraft is due to viscous drag.

In two-dimensional boundary layers, the fundamental instability mode is the Tollmien–Schlichting (T-S) wave, named after Tollmien [3] and Schlichting [4]. For transition prediction, van Ingen [5] and Smith and Gamberoni [6] independently proposed a semi-empirical method based on linear stability theory, known as the e^N method. However, other transition mechanisms may occur, such as transient growth or bypass transition [7]. Many studies investigate the effect of surface imperfections on T-S wave amplification. Perraud et al. [8] compared variations in the N factor (ΔN) computed via T-S wave growth in boundary layers with and without a gap. Forte et al. [9] conducted an experimental study to validate the model proposed by Perraud et al. [10], providing evidence of bypass transition. Beguet et al. [11] identified the limits for bypass conditions based on gap length and depth normalized by the displacement thickness, with $L/\delta^* \geq 18$ and $D/\delta^* \geq 2$, respectively. Crouch and Kosorygin [12] conducted experimental studies correlating step, regular protrusion, and gap effects on boundary layer transition. Crouch et al. [13] also presented experimental ΔN correlations for cavity-induced transition for different cavity sizes. In one particular case where bypass transition occurred, they observed a frequency higher than expected for the unstable T-S range in that flow configuration. Zahn and Rist [14] numerically studied the influence of deep gaps on boundary layer transition by comparing T-S wave growth (ΔN) in flows with and without gaps. They concluded that a stationary acoustic wave inside the gap significantly affected the growth of T-S waves. Mathias and Medeiros [15] compared the spatial evolution of wavepackets over a gap and a smooth flat plate under the same conditions. The wavepackets exhibited local distortion over the gap, which attenuated further downstream, except for a phase shift. The frequency spectrum revealed increased amplitude at higher frequencies, while the effect was negligible in the lower frequency range.

Early investigations reported the presence of instabilities associated with cavity flows, as noted by Krishnamurty [16], Plumblee et al. [17], and Rossiter [18]. The latter empirically proposed a physical mechanism explaining acoustic radiation characterized by distinct frequencies. Vortices shed from the cavity leading edge collide with the trailing edge, generating acoustic waves that destabilize the mixing layer at the leading edge, thus closing the feedback loop. Sarohia [19] performed experiments to determine the threshold for the onset of cavity oscillations. Yamouni et al. [20] conducted global stability analyses and observed amplification overshoots of unstable Rossiter modes when interacting with standing waves described by Plumblee et al. [17]. Mathias and Medeiros [21] studied the influence of Mach number and displacement thickness on gap stability, concluding that the incoming boundary layer influences the selection of Rossiter modes, while the Mach number enhances both acoustic energy transfer and temporal growth rate. Furthermore, cavity flows exhibit three-dimensional oscillatory modes associated with centrifugal instability. Brés and Colonius [22] numerically investigated the stability of three-dimensional perturbations in two-dimensional cavity flows. Their results showed unstable modes with wavelengths on the order of the cavity depth, differing in frequency range. They attributed this instability to a non-acoustic centrifugal mechanism. The mode showed low sensitivity to Mach number but was influenced by Reynolds number, which affected instability and mode hierarchy. De Vicente et al. [23] and Meseguer-Garrido et al. [24] analyzed centrifugal instability in regimes without Rossiter modes, producing neutral stability diagrams and amplification curves for different spanwise wavenumbers and Reynolds numbers. Sun et al. [25] compared results from linear stability analysis and three-dimensional DNS, warning that cavities with large aspect ratios showed strong nonlinear interactions between 2D and 3D modes, which deviated from linear theory predictions. Mathias and de Medeiros [26] numerically investigated interactions between Rossiter and centrifugal modes. In 3D simulations, the Rossiter-related spectral peaks were broader compared to 2D simulations. The authors attributed this to spanwise modulation of Rossiter modes caused by centrifugal instabilities, which could potentially alter the base flow and its stability. Victorino et al. [27] computationally identified a link between bypass transition and unstable cavity modes, such as Rossiter and centrifugal instabilities. In their DNS study, nonlinear interaction between centrifugal and Rossiter modes led to transition.

III. Methodology

We use Direct Numerical Simulation (DNS) and a time-stepping algorithm based on the Arnoldi method [28] to approximate the eigenvalues and eigenfunctions for modal analysis. Both codes were developed in-house and are open-source*. The DNS solves the compressible Navier–Stokes Equations (NSE), given by Eqs. 1, 2, 3, 4, and 5.

$$\frac{\partial \rho}{\partial t} = -\rho \frac{\partial u_i}{\partial x_i} - u_i \frac{\partial \rho}{\partial x_i} \tag{1}$$

$$\frac{\partial u_j}{\partial t} = -u_i \frac{\partial u_j}{\partial x_i} - \frac{1}{\rho}\frac{\partial p}{\partial x_j} + \frac{1}{\rho}\frac{\partial \tau_{ij}}{\partial x_i} \tag{2}$$

$$\frac{\partial e}{\partial t} = u_i \frac{\partial e}{\partial x_i} - \frac{p}{\rho}\frac{\partial u_i}{\partial x_i} + \frac{\tau_{ij}}{\rho}\frac{\partial u_j}{\partial x_i} - \frac{1}{\rho}\frac{\partial q_i}{\partial x_i} \tag{3}$$

Where the viscous stress tensor and heat flux are defined as:

$$\tau_{ij} = \frac{\mu}{Re}\left(\frac{\partial u_i}{\partial x_j} + \frac{\partial u_j}{\partial x_i} - \frac{2}{3}\delta_{ij}\frac{\partial u_k}{\partial x_k}\right) \tag{4}$$

$$q_i = -\frac{\mu}{(\gamma - 1)\, Re\, Pr\, Ma^2}\frac{\partial T}{\partial x_i} \tag{5}$$

Scalar quantities such as density ρ, energy e, temperature T, and pressure p are used, while the velocity vector is represented as $\vec{V} = u\hat{i} + v\hat{j} + w\hat{k}$. All variables are non-dimensionalized using reference scales. The non-dimensional parameters Re, Pr, and M represent the Reynolds, Prandtl, and Mach numbers, respectively. The computational domain is defined using a Cartesian, structured, and stretched mesh. Buffer zones are applied near open boundaries to damp reflective oscillations by increasing node spacing and lowering the spatial accuracy order. Spatial derivatives are approximated using a spectral-like scheme based on [29] and [30]. A spatial anti-aliasing filter adapted from [31] is used to suppress unresolved motion. Time integration is carried out using a fourth-order Runge–Kutta method.

The upstream boundary condition assumes uniform flow with constant energy and zero streamwise pressure gradient. Outlet and outflow boundaries are imposed with zero second derivatives and a prescribed pressure. At the bottom boundary, a free-slip wall model is used with zero streamwise wall-normal velocity gradient ($\partial U/\partial y$). The flat plate is maintained at a constant isothermal condition, with no-slip and no-penetration conditions applied to the velocity field. A zero normal pressure gradient is also enforced. For globally unstable flows, selective frequency damping can be activated inside the domain following [32], enabling convergence to a time-invariant base flow. Domain decomposition for parallel execution follows the method described in [33].

Due to the strong non-parallel effects in the flow over the gap, linear stability analysis is performed using the global stability approach. The eigenvalues and corresponding eigenfunctions of the Jacobian matrix are approximated using a time-stepping method based on [28, 34]. In summary, a small perturbation is added to a previously obtained base flow, and the DNS solver is iteratively run for a fixed time. After each iteration, a new orthogonal disturbance is generated for the next step, contributing a new column to the upper Hessenberg matrix H. After sufficient iterations, the complex eigenvalues and eigenvectors of H closely approximate those of the original system. The real part of the eigenvalues represents temporal growth—positive values indicate instability—while the imaginary part corresponds to the circular frequency of the mode. The eigenfunction captures the spatial structure of the mode at a particular phase. For details on the implementation, accuracy, validation, and input parameters, refer to [35].

IV. Results

A. Three-dimensional flow

A three-dimensional simulation was conducted using the parameters shown in Table 1. This case was selected because it allowed the identification of distinct regions of interest. These regions are as follows: the inlet region upstream of the cavity, which is not relevant for analysis as the flow is laminar and only acoustic waves are present from the cavity; the gap region, which is of particular interest due to the presence of flow structures that are convected

*https://github.com/marlonsmathias/GATT_DNS

Table 1 Case parameters.

Parameter	Value
Re_{δ^*}	734
Ma	0.5
D/δ^*	6.11
L/δ^*	12.22
L/D	2
Number of Snapshots	13000

downstream; the transition region, starting from the cavity's trailing edge to where turbulence develops; and finally, the region of fully developed turbulence.

Figure 1 shows these four regions using isosurfaces of λ_2, colored by turbulent kinetic energy production. Figure 2 presents the friction coefficient, calculated using a time average in the spanwise direction. In Fig. 1, both two- and three-dimensional structures are visible within the cavity, as well as two-dimensional structures convected downstream. These structures eventually break down into Λ vortices and evolve into turbulent flow.

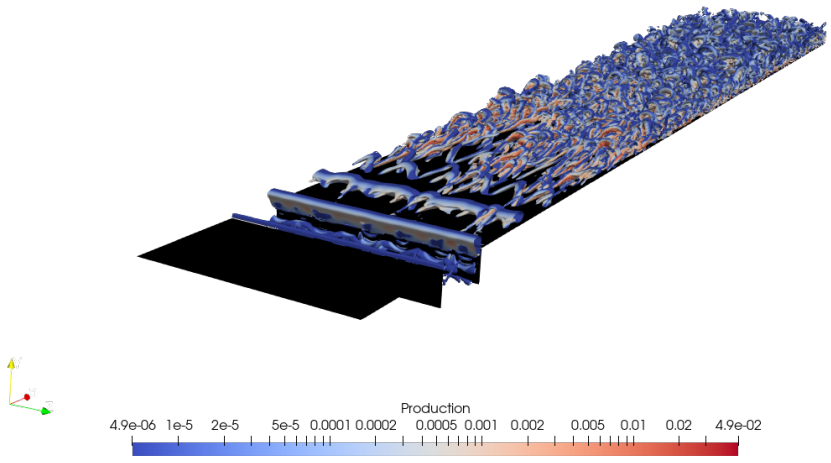

Fig. 1 Isosurface using the λ_2 criterion, colored by turbulent kinetic energy production at a given time step.

By analyzing the behavior of C_f in Fig. 2, we observe a region where the flow stabilizes and progresses toward fully developed turbulence. This behavior suggests a possible memory effect from the modes within the cavity, influencing part of the turbulent region.

Based on these observations, linear stability analysis was performed using the group's biglobal solver. In addition, Spectral Proper Orthogonal Decomposition (SPOD) was employed to analyze the modal content of the flow. A total of 13,000 snapshots of the three-dimensional flow were used in this analysis.

B. Comparison Between LST Prediction and SPOD Modes

To investigate the modes potentially present in the cavity, biglobal linear stability theory (LST) was applied. The spanwise wavenumber was scanned from 0 to π, in increments of 0.1π. For the two-dimensional case ($k_z = 0$), only one

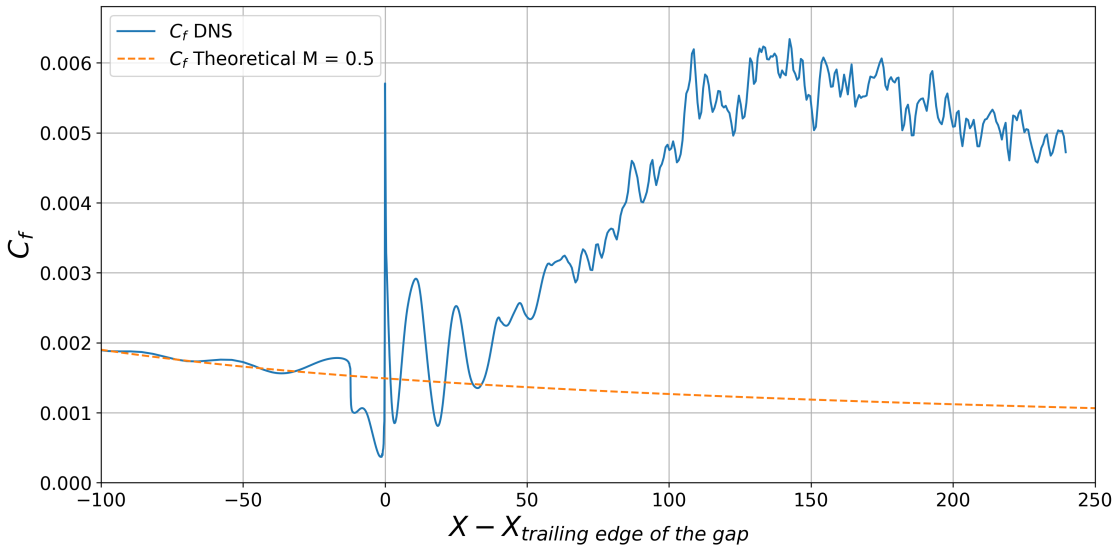

Fig. 2 Comparison of the friction coefficient obtained from time-averaged and spanwise-averaged values, alongside theoretical predictions for laminar and turbulent cases.

unstable mode—a Rossiter mode of type I—was found. For the three-dimensional case, three types of centrifugal modes described by Brés and Colonius [22] were identified. The dominant mode was centrifugal type I, followed by type III.

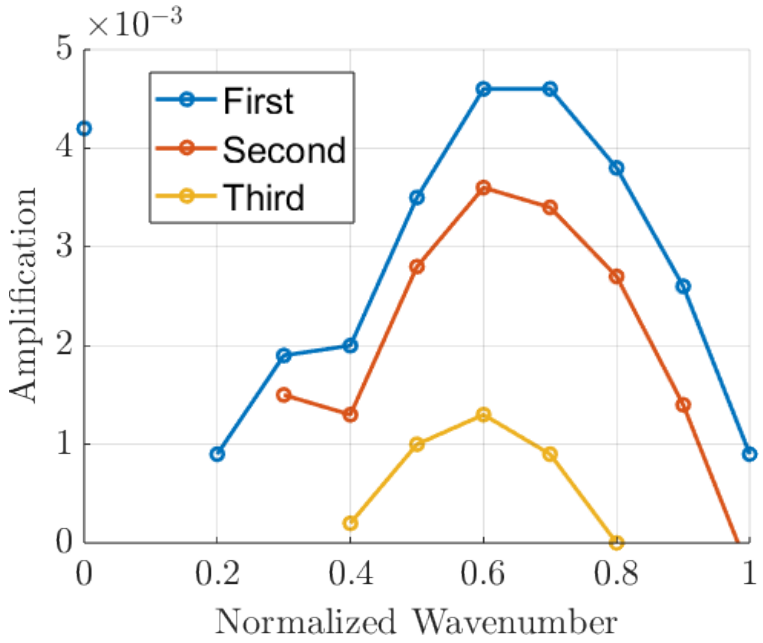

Fig. 3 Growth rate of the most unstable mode for each spanwise wavenumber predicted by LST.

Figure 4 shows three distinct frequency bands, clearly identifying the three centrifugal modes. The most unstable modes are the stationary (centrifugal type I) and the second non-stationary (centrifugal type III). Time-frequency analysis was used to focus on these non-stationary modes.

SPOD [36, 37] was applied to the three-dimensional flow to analyze the flow's limit cycle and compare it with the modes predicted by theory. For this, 13,000 snapshots were analyzed, considering the first 20 spanwise wavenumbers. These modes contain over 85% of the total flow energy, making them representative for preliminary analysis. Figure 5 shows the frequency spectra of the most energetic mode at each frequency.

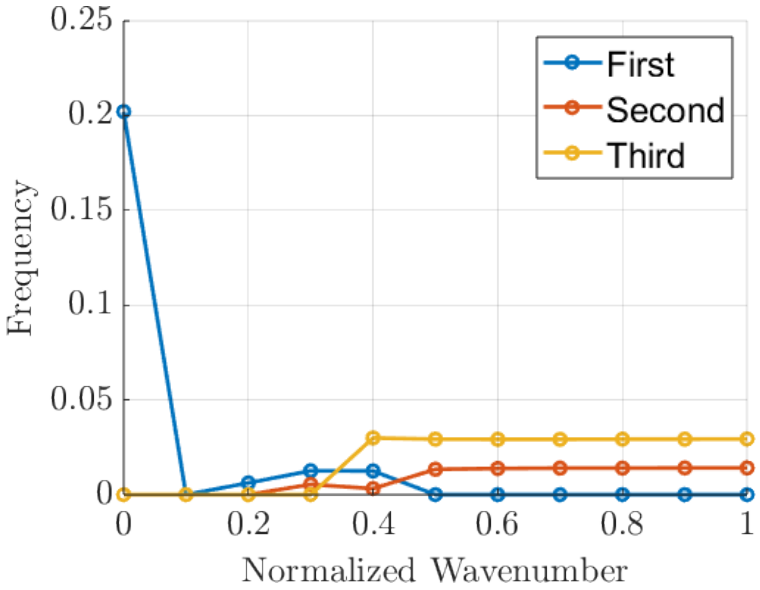

Fig. 4 Frequency of the most unstable mode for each spanwise wavenumber predicted by LST.

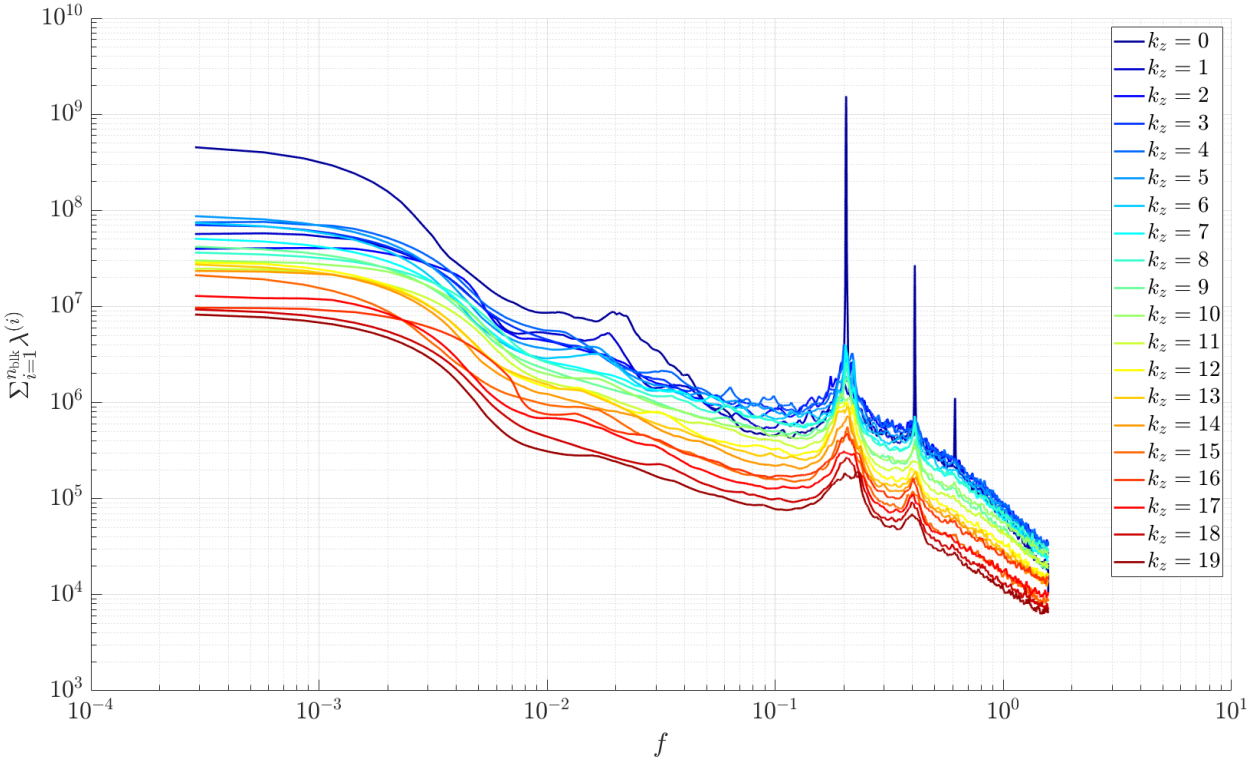

Fig. 5 SPOD energy spectrum of the most energetic mode for each frequency, computed for the first twenty spanwise wavenumbers.

The spectrum reveals a mode at the same frequency as the Rossiter type I predicted by LST. Additionally, its first two harmonics are present. For non-zero wavenumbers, energy peaks are observed around the Rossiter frequency and its harmonics. At lower frequencies, energy peaks appear near the predicted region of the centrifugal modes. For $k_z > 10$, an inflection in the energy spectrum suggests a change in modal dynamics in the frequency range $10^{-2} < f < 10^{-1}$.

Focusing now on eigenfunctions, Fig. 6 presents the LST-predicted Rossiter type I mode for the V component. The linear theory predicts the highest energy concentration within the cavity, with a residual effect extending about five cavity lengths downstream.

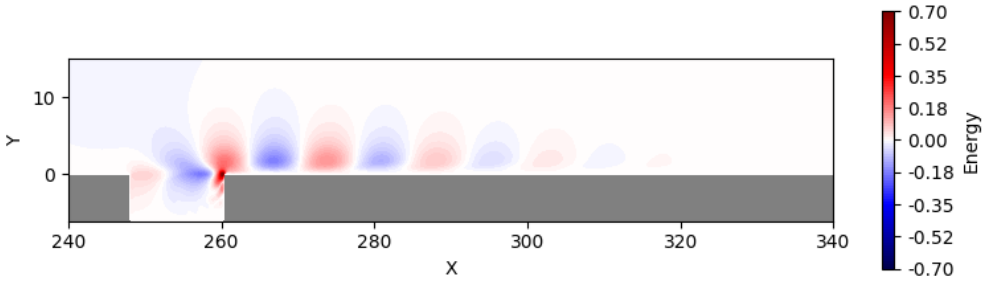

Fig. 6 Eigenfunction of Rossiter mode I obtained via LST for the V component.

The SPOD-derived counterpart is shown in Fig. 7, exhibiting similar spatial structures. However, it shows a more extended memory of the Rossiter mode into the transition region and even into the turbulent region. This suggests that the Rossiter mode contributes to the boundary layer transition process. Nevertheless, being two-dimensional, additional mechanisms are required to induce the observed three-dimensional turbulence.

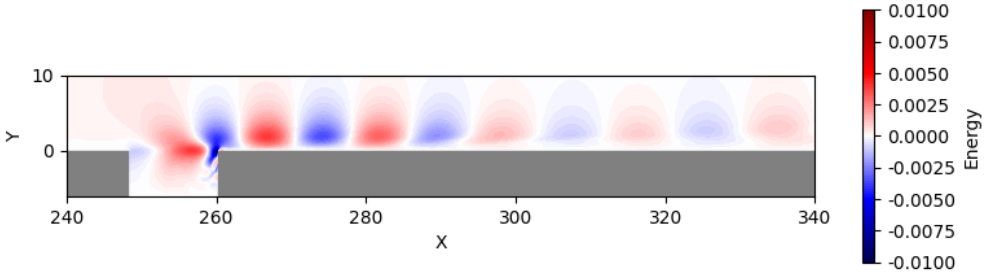

Fig. 7 Eigenfunction of Rossiter mode I obtained via SPOD for the V component.

Moving on to the three-dimensional modes, LST predicts centrifugal modes characterized by internal cavity recirculation. Figure 8 shows the eigenfunction of the most unstable non-stationary centrifugal mode. The energy is primarily confined within the gap, with a small portion convected downstream.

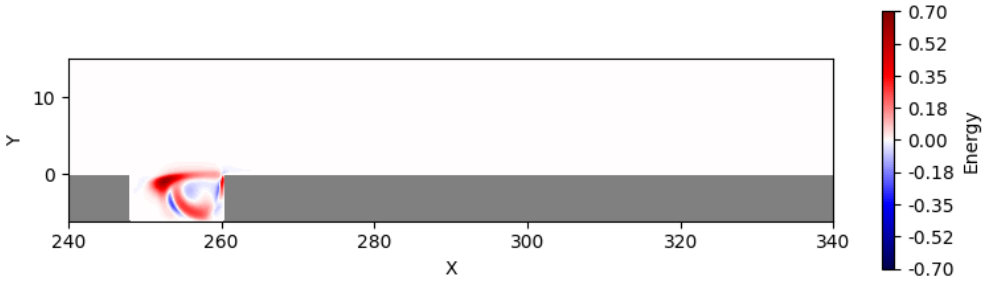

Fig. 8 Eigenfunction of the most unstable non-stationary centrifugal mode obtained via LST for the V component.

Figure 9 presents the corresponding SPOD result. The energy remains mostly inside the gap, with a small wake being convected downstream. However, the spatial shape of the mode appears more deformed compared to the LST result.

The interaction between Rossiter and centrifugal modes may lead to secondary instabilities, contributing to boundary layer transition. However, fully understanding this process requires further investigation.

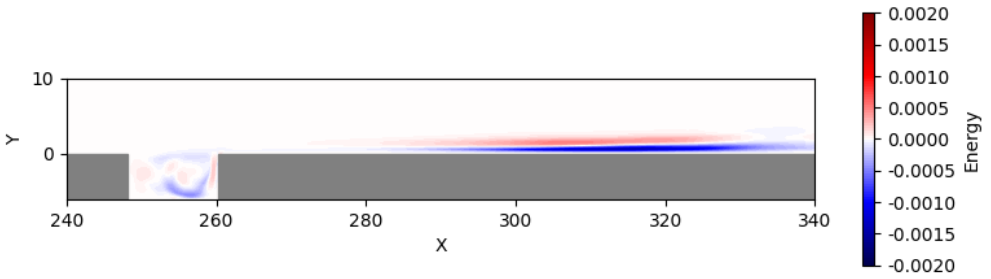

Fig. 9 Eigenfunction of the most unstable non-stationary centrifugal mode obtained via SPOD for the V component.

V. Conclusion

The literature indicates that cavities can anticipate the boundary layer transition process. Both two-dimensional and three-dimensional instability modes associated with cavities have been observed, particularly Rossiter and centrifugal modes.

To investigate cavity-induced transition, a cavity with an aspect ratio of 2 was selected under subsonic Mach number conditions. Using linear stability theory, several modes were predicted, including Rossiter mode I and both stationary and non-stationary centrifugal modes.

A DNS of the same configuration was performed, generating 13,000 snapshots, which enabled SPOD to be applied with high frequency resolution. In this case, transition of the boundary layer downstream of the gap was observed, with Λ vortices developing from structures convected out of the cavity.

SPOD analysis revealed several modes whose frequencies aligned with those predicted by linear theory, enabling the extraction and comparison of eigenfunctions. The Rossiter mode eigenfunctions obtained from both LST and SPOD were similar. The main difference was downstream of the cavity, where the SPOD-based eigenfunction exhibited high energy content in the transition region and retained memory into the turbulent region.

For the centrifugal modes, only non-stationary modes were analyzed, and comparable frequencies were found. Unlike Rossiter modes, the centrifugal mode eigenfunctions showed deformation and a convected wake emerging from the cavity.

The presence of Rossiter mode memory in the transitional and turbulent regions suggests its contribution to boundary layer transition. However, as a two-dimensional mode, some form of three-dimensionalization is necessary for turbulence to fully develop. A potential mechanism for this could be the interaction with centrifugal modes. Further studies will be conducted to deepen the understanding of this transition mechanism.

Acknowledgments

We would like to thank the Coordenação de Aperfeiçoamento de Pessoal de Nível Superior (CAPES)- Programa de Excelência Acadêmica (PROEX) - Brasil for Financial Support. M.A.F.M. is sponsored by CNPq/Brazil (grant no.307956/2019-9), sponsored by FAPESP (grant no. 2019/15336-7) and the US Air Force Office of Scientific Research (AFOSR) for grant FA9550-18-1-0112 and FA9550-23-1-0030, managed by Dr. Daniel Montes and Dr. Roger Greenwood; the Center for Mathematical Sciences Applied to Industry (CeMEAI) funded by São Paulo Research Foundation (FAPESP/Brazil), grant 2013/07375-0, for access to the Euler cluster, led by Prof. José Alberto Cuminato. This work used resources of the "Centro Nacional de Processamento de Alto Desempenho em São Paulo (CENAPAD-SP). OTS thankfully acknowledges support by AFOSR grant no. FA9550-22-1-0541 with Dr. Gregg Abate as the Program Officer.

References

[1] Schneider, W., "The Importance of Aerodynamics in the Development of Commercially Successful Transport Aircraft," *Aerodynamic Drag reduction technologies: proceedings of the CEAS, DragNet European Drag Reduction Conference 19 - 21 June 2000, Potsdam, Germany*, 2001, pp. 9–16.

[2] Marec, J.-P., "Drag reduction: a major task for research," *Aerodynamic Drag reduction technologies: proceedings of the CEAS, DragNet European Drag Reduction Conference 19 - 21 June 2000, Potsdam, Germany*, 2001, pp. 17 – 28.

[3] Tollmien, W., "The production of turbulence," *National Advisory Committee for Aeronautics - Technical Memorandum no. 609*, 1931.

[4] Schlichting, H., "Laminare Strahlausbreitung," *ZAMM - Journal of Applied Mathematics and Mechanics / Zeitschrift für Angewandte Mathematik und Mechanik*, Vol. 13, No. 4, 1933, pp. 260–263. https://doi.org/10.1002/zamm.19330130403.

[5] van Ingen, J. L., "A suggested semi-empirical method for calculation of the boundary layer transition region," *Technische Hogeschool Vliegtuigbouwkunde - Report V.T.H.-74*, 1956.

[6] Smith, A. M. O., and Gamberoni, N., "Transition, Pressure Gradient, and Stability Theory," Tech. Rep. ES 26388, Douglas Aircraft Division, 1956. URL https://engineering.purdue.edu/~aae519/BAM6QT-Mach-6-tunnel/otherpapers/smith-amo-eN-douglas-es26388-1956.pdf.

[7] Saric, W. S., Reed, H. L., and Kerschen, E. J., "BOUNDARY-LAYER RECEPTIVITY TO FREESTREAM DISTURBANCES," *Annual Review of Fluid Mechanics*, Vol. 34, No. 1, 2002, pp. 291–319. https://doi.org/10.1146/annurev.fluid.34.082701.161921, URL https://doi.org/10.1146/annurev.fluid.34.082701.161921.

[8] Perraud, J., Arnal, D., Séraudie, A., and Tran, D., "Laminar-Turbulent Transition on Aerodynamic Surfaces with Imperfections," *RTO-AVT-111 Symposium*, October 2004, pp. 4–7. https://doi.org/10.13140/RG.2.1.3532.1364.

[9] Forte, M., Perraud, J., Seraudie, A., Beguet, S., and Casalis, L. G. G., "Experimental and Numerical Study of the Effect of Gaps on Laminar Turbulent Transition of Incompressible Boundary Layers," *Procedia IUTAM*, Vol. 14, No. 0, 2015, pp. 448–458. https://doi.org/10.1016/j.piutam.2015.03.073, URL http://dx.doi.org/10.1016/j.piutam.2015.03.073.

[10] Perraud, J., Arnal, D., and Kuehn, W., "Laminar-turbulent transition prediction in the presence of surface imperfections," *International Journal of Engineering Systems Modelling and Simulation*, Vol. 6, No. 3-4, 2014, pp. 162–170. https://doi.org/10.1504/IJESMS.2014.063129.

[11] Beguet, S., Perraud, J., Forte, M., and Brazier, J. P., "Modeling of transverse gaps effects on boundary-layer transition," *Journal of Aircraft*, Vol. 54, No. 2, 2017, pp. 794–801. https://doi.org/10.2514/1.C033647.

[12] Crouch, J. D., and Kosorygin, V. S., "Surface Step Effects on Boundary-Layer Transition Dominated by Tollmien–Schlichting Instability," *AIAA Journal*, Vol. 58, No. 7, 2020, pp. 2943–2950. https://doi.org/10.2514/1.j058518.

[13] Crouch, J., Kosorygin, V., Sutanto, M., and Miller, G., "Characterizing surface-gap effects on boundary-layer transition dominated by Tollmien–Schlichting instability," *Flow*, Vol. 2, No. E8, 2022. URL http://doi:10.1017/flo.2022.1.

[14] Zahn, J., and Rist, U., "Impact of deep gaps on laminar - Turbulent transition in compressible boundary-layer flow," *AIAA Journal*, Vol. 54, No. 1, 2016, pp. 66–76. https://doi.org/10.2514/1.J054112.

[15] Mathias, M. S., and Medeiros, M. A. F., "Global instability analysis of a boundary layer flow over a small cavity," *AIAA Aviation 2019 Forum 17-21 June 2019, Dallas, Texas*, 2019.

[16] Krishnamurty, K., "Acoustic radiation from two-dimensional rectangular cutouts in aerodynamic surfaces," Technical Note 3487, National Advisory Committee for Aeronautics, Washington, US, Aug. 1955. URL https://digital.library.unt.edu/ark:/67531/metadc57843/.

[17] Plumblee, H. E., Gibson, J. S., and Lassiter, L. W., "Theoretical and Experimental Investigation of The Acoustic Response of Cavities In An Aerodynamic Flow," *Technical Report USAF Report WADD-TR-61-75*, 1962, pp. 1–167.

[18] Rossiter, J. E., "Wind-tunnel experiments on the flow over rectangular cavities at subsonic and transonic speeds," *Reports and Memoranda No. 3438 - Aeronautical Research Council - Ministry of Aviation*, 1964.

[19] Sarohia, V., "Experimental investigation of oscillations in flows over shallow cavities," *AIAA Journal*, Vol. 15, No. 7, 1977, pp. 984–991. https://doi.org/10.2514/3.60739.

[20] Yamouni, S., Sipp, D., and Jacquin, L., "Interaction between feedback aeroacoustic and acoustic resonance mechanisms in a cavity flow: A global stability analysis," *Journal of Fluid Mechanics*, Vol. 717, 2013, pp. 134–165. https://doi.org/10.1017/jfm.2012.563.

[21] Mathias, M. S., and Medeiros, M. A. F., "The effect of incoming boundary layer thickness and Mach number on linear and nonlinear Rossiter modes in open cavity flows," *Theor. Comput. Fluid Dyn.*, Vol. 35, No. 4, 2021, pp. 495–513.

[22] Brés, G. A., and Colonius, T., "Three-dimensional instabilities in compressible flow over open cavities," *Journal of Fluid Mechanics*, Vol. 599, 2008, pp. 309–339. https://doi.org/10.1017/S0022112007009925.

[23] De Vicente, J., Basley, J., Meseguer-Garrido, F., Soria, J., and Theofilis, V., "Three-dimensional instabilities over a rectangular open cavity: From linear stability analysis to experimentation," *Journal of Fluid Mechanics*, Vol. 748, 2014, pp. 189–220. https://doi.org/10.1017/jfm.2014.126.

[24] Meseguer-Garrido, F., De Vicente, J., Valero, E., and Theofilis, V., "On linear instability mechanisms in incompressible open cavity flow," *Journal of Fluid Mechanics*, Vol. 752, 2014, pp. 219–236. https://doi.org/10.1017/jfm.2014.253.

[25] Sun, Y., Taira, K., Cattafesta, L. N., and Ukeiley, L. S., "Biglobal instabilities of compressible open-cavity flows," *Journal of Fluid Mechanics*, Vol. 826, 2017, pp. 270–301. https://doi.org/10.1017/jfm.2017.416.

[26] Mathias, M. S., and de Medeiros, M. A. F., "Interaction between rossiter and görtler modes in the compressible flow in an open cavity," *Aiaa Aviation 2020 Forum*, Vol. 1 PartF, 2020, pp. 1–6. https://doi.org/10.2514/6.2020-3074.

[27] Victorino, V. B., Aguirre, F. O., and de Medeiros, M. A. F., "Gap induced boundary layer transition," *AIAA AVIATION Forum*, 2023, pp. 1–14.

[28] Arnoldi, W. E., "The principle of minimized iterations in the solution of the matrix eigenvalue problem," *Quarterly of Applied Mathematics*, Vol. 9, 1951, pp. 17–29.

[29] Lele, S. K., "Compact Finite and Difference Schemes and with Spectral-like and Resolution," *Journal of Computational physics*, Vol. 103, 1992, pp. 16–42.

[30] Gaitonde, D., and Shang, J. S., "High-order finite-volume schemes in wave propagation phenomena," *27th Plasma Dynamics and Lasers Conference*, June 1996. https://doi.org/10.2514/6.1996-2335.

[31] Gaitonde, D. V., and Visbal, M. R., "High-Order Schemes for Navier-Stokes Equations: Algorithm and Implementation Into FDL3DI," Technical Report 1998-3060, AIR FORCE RESEARCH LAB WRIGHT-PATTERSON, Jul. 1998. URL https://apps.dtic.mil/sti/citations/ADA364301.

[32] Åkervik, E., Brandt, L., Henningson, D. S., Hœpffner, J., Marxen, O., and Schlatter, P., "Steady solutions of the Navier-Stokes equations by selective frequency damping," *Physics of Fluids*, Vol. 18, No. 6, 2006, p. 068102. https://doi.org/10.1063/1.2211705.

[33] Li, N., and Laizet, S., "2DECOMP&FFT - A Highly Scalable 2D Decomposition Library and FFT Interface," Tech. rep., Numerical Algorithms Group (NAG) - Imperial College London, 2010.

[34] Tezuka, A., and Suzuki, K., "Three-dimensional global linear stability analysis of flow around a spheroid," *AIAA Journal*, Vol. 44, No. 8, 2006, pp. 1697–1708. https://doi.org/10.2514/1.16632.

[35] Mathias, M. S., "Computational study of the hydrodynamic stability of gaps and cavities in a subsonic compressible boundary layer," Ph.D. thesis, São Carlos School of Engineering, University of São Paulo, 2021.

[36] Towne, A., Schmidt, O. T., and Colonius, T., "Spectral proper orthogonal decomposition and its relationship to dynamic mode decomposition and resolvent analysis," *Journal of Fluid Mechanics*, Vol. 847, 2018, p. 821–867. https://doi.org/10.1017/jfm.2018.283.

[37] Schmidt, O. T., and Colonius, T., "Guide to Spectral Proper Orthogonal Decomposition," *AIAA Journal*, Vol. 58, No. 3, 2020, pp. 1023–1033. https://doi.org/10.2514/1.J058809, URL https://doi.org/10.2514/1.J058809.